NANO LETTERS

LETTER

pubs.acs.org/NanoLett

Plasmon Resonance in Individual Nanogap Electrodes Studied Using Graphene Nanoconstrictions as Photodetectors

S.-F. Shi,[†] Xiaodong Xu,[†,‡] D. C. Ralph,*[,†,§] and P. L. McEuen[†,§]

[†]Physics Department, Cornell University, Ithaca, New York 14853, United States

[‡]Department of Physics, University of Washington, Seattle, 98195, United States

[§]Kavli Institute at Cornell, Cornell University, Ithaca, New York 14853, United States

ABSTRACT: We achieve direct electrical readout of the wavelength and polarization dependence of the plasmon resonance in individual gold nanogap antennas by positioning a graphene nanoconstriction within the gap as a localized photodetector. The polarization sensitivities can be as large as 99%, while the plasmon-induced photocurrent enhancement is 2−100. The plasmon peak frequency, polarization sensitivity, and photocurrent enhancement all vary between devices, indicating the degree to which the plasmon resonance is sensitive to nanometer-scale irregularities.

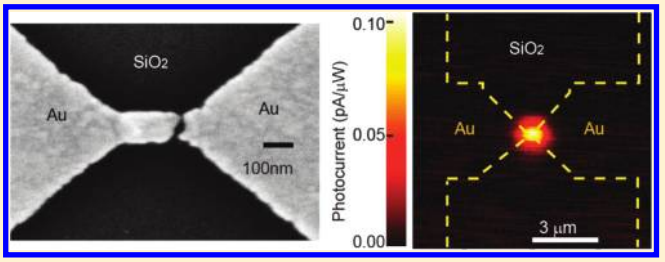

KEYWORDS: Plasmon, graphene, photocurrent, nanoribbon

Plasmonic nanostructures can act as optical antennas,[1,2] concentrating incident light energy into a nanoscale volume with dimensions much smaller than the light wavelength and thereby greatly enhancing the strength of the optical-frequency electric field. This enhanced optical field has been used for single molecule Raman spectroscopy,[3−5] second (and higher) harmonic generation,[6−8] and fluorescence enhancement.[9−11] Here we explore a strategy to achieve direct electrical readout of plasmon-enhanced optical fields, which is challenging because the region of field enhancement is so small. Specifically, we use a self-aligned fabrication process to couple a gold break junction acting as a plasmonic antenna with a sub-10 nm graphene constriction, whose nonlinear electrical characteristics allow it to serve as a photodetector. Our dual goals are to use the nanoscale photodetector to characterize the enhanced optical field produced by the plasmon and also to understand the mechanism that allows graphene constrictions to generate photocurrent (PC). Our results go beyond previous studies of PC in metal break junctions[12] in that we directly measure the size of the plasmon enhancement by recording the wavelength dependence of the resonantly enhanced PC and observe that the PC is strongly modulated by the polarization direction of the incident light, with significant differences in peak frequency and polarization sensitivity between devices. The sign of the photocurrent also differs between devices but is always the same as the second derivative of the low-frequency current−voltage curve, allowing us to associate the mechanism of the photocurrent with optical rectification. The plasmon-induced enhancement of the photocurrent varies from a factor of 2 to 100 in different samples.

Our devices consist of a graphene constriction positioned within a sub-10 nm scale gap between two gold electrodes. We first grow the graphene by chemical vapor deposition[13] on Cu foil, transfer the graphene with a PMMA backing onto an oxidized Si wafer, remove the PMMA by soaking in acetone overnight, and prepattern the graphene using photolithography and oxygen-plasma etching into 20 × 100 μm^2 strips. Micro-Raman spectroscopy was used to confirm that the graphene was single layer. We use two stages of electron-beam lithography and lift-off to deposit 100 nm wide wires made from 1 nm Ti/20 nm Au on top of the graphene, connected to wider 3 nm Ti/100 nm Au contacts. We then use oxygen plasma to etch away the graphene everywhere except under the Au (inset, Figure 1). To fabricate nanoscale constrictions, we employ two steps of electromigration. In the first step, we use electromigration with electronic feedback[14] at room temperature in air to break the Au wire and leave a nanoscale gap (Figure 1a) that will correspond to the high-electric-field region of the plasmonic antenna. This process requires maximum voltages on the order of 0.5 V for which the 100 nm wide graphene layer underneath the Au remains conducting (resistances $R < 20$ kΩ). We then narrow the graphene wire into a nanoconstriction (Figure 1b) without breaking it fully using a second stage of electromigration in vacuum, similar to previous experiments by other groups.[15−17] Because graphene nanoribbons can sustain much higher current density than Au,[18] this requires much larger voltages, 2−5 V, consistent with previous reports.[19]

Figure 1c shows current−voltage ($I-V$) curves at 4.2 K as a graphene junction is progressively narrowed by repeated electromigration. After the first stage of electromigration of just the gold wire (leaving the graphene intact), the $I-V$ curve has a simple linear form (inset, Figure 1c). After subsequent electromigration of the graphene, the $I-V$ characteristics become nonlinear with a

Received: February 13, 2011
Revised: March 14, 2011
Published: March 24, 2011

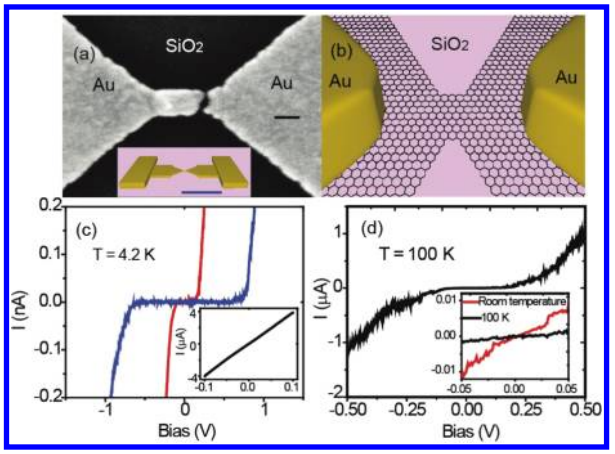

Figure 1. (a) Scanning electron microscope picture of a Au/graphene device after the Au wire is broken by electromigration. Scale bar is 100 nm. (inset) Geometry of the Au electrodes and larger contact pads. Scale bar in inset is 5 μm. (b) Artist's conception of a device structure after a second stage of electromigration is used to create a graphene nanoconstriction in the nanogap between gold electrodes. (c) Current−voltage curves for device 8 at 4.2 K after two stages of electromigration that progressively narrowed the graphene constriction and increased the transport gap. (inset) Current−voltage curve for the same device at 4.2 K after the gold wire was broken by electromigration, but before any electromigration of the graphene. (d) Current−voltage curve of device 6 at 100 K and (inset) at room temperature. At high bias, the curves are noisy due to resistance fluctuations.

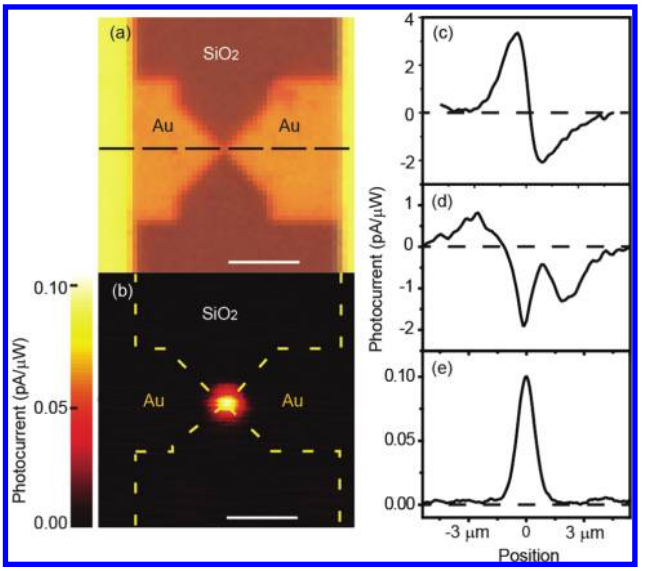

Figure 2. (a) Reflected light image of a typical device. The dashed line denotes the centerline of the Au electrodes, the orientation of the scans in panels (c−e). Scale bar is 3 μm. (b) Photocurrent response as a function of laser spot position for device 6. Scale bar is 3 μm. (c−e) Photocurrent response at 780 nm as a function of laser position for (c) a 100 nm wide graphene ribbon with room-temperature resistance $R = 8$ kΩ, (d) a 100 nm wide graphene ribbon with $R = 10$ kΩ, and (e) device 6, a graphene nanoconstriction with $R = 5$ MΩ. These panels show the evolution from an antisymmetric thermal PC response to a symmetric rectification response. The symmetric rectification signal can be positive or negative.

region of low current near zero bias whose width in source-drain bias increases with each additional step of electromigration (Figure 1c, main panel). Figure 1d shows the $I-V$ curves for a different device on which photocurrent measurements were performed. The zero-bias resistance at low temperature (100 K) is $R \sim 100$ MΩ, with a turn-on of current near $V = \pm 0.2$ V. At room temperature (inset in Figure 1d), the nonlinearities in the $I-V$ curve are smaller than at low temperature and the zero-bias resistance is ∼5 MΩ. The $I-V$ characteristics in Figure 1c,d are similar to previous transport studies of nanoscale graphene constrictions fabricated by electron-beam lithography,[20−27] by chemical preparation of nanoribbons,[28] and by electromigration.[15−17] Lateral patterning and the associated formation of localized states leads to an energy gap for electron transport in graphene that suppresses conduction at low voltage and low temperature.[26,27] Because our constrictions are short, the large gap as a function of source−drain voltage (>0.1 V) that we observe implies that the constriction width for the graphene in our samples is significantly less than 10 nm.[16,17,22,29] The final device structure therefore allows the graphene to measure the optical intensity in a much smaller region than, for example, previous Ge-based photodetectors integrated into infrared dipole antennas with 60 nm gaps.[30] Our devices also have much smaller conductance (0.001−1 e^2/h) than the scale required to short out the plasmon resonance mode (∼tens of e^2/h),[31] so we expect the graphene to produce negligible perturbation to the plasmon properties.

We perform photocurrent (PC) measurements using a Ti-sapphire tunable continuous wave laser source focused to a 1.2 μm spot size with incident power ranging from 1 μW to 1 mW. We measure the PC and the reflected light simultaneously as we scan the position of the laser spot. A reflection image of a graphene device with Au nanogap electrodes is shown in Figure 2a. For scans along the centerline of the electrodes (the dotted line in Figure 2a), we find that the PC response can differ qualitatively depending on the device resistance and the width of the graphene. For low-resistance devices (with room-temperature $R = 5-20$ kΩ, corresponding to 100 nm wide graphene nanoribbons after the gold electrodes are broken by electromigration (but before the electromigration of the graphene), we observe two types of PC. One is a PC that antisymmetric in sign about the position of the nanocontact with the largest signal magnitudes for laser spot positions within the Au electrodes, approximately 0.5 μm away from the contact (Figure 2c). The other type of signal is an antisymmetric PC superimposed together with a symmetric peak (with either positive or negative sign) centered at the position of the graphene constriction (Figure 2d). In contrast, the antisymmetric signals are absent for the sub-10 nm graphene constrictions (with room-temperature $R > 50$ kΩ), leaving only the symmetric-in-position PC peak with a sign that varies from device to device (Figure 2e). The PC in this case is observable only when the laser spot overlaps the narrowest region of the break junction device (Figure 2b). PC signals that are antisymmetric as a function of position along the electrodes have been observed previously for contacts to large-area graphene and have been explained as due to heating in the electrodes.[32,33] This heating contribution is expected[34] to take the form $I = [2\pi^2 e k_B^2 T/(3h)]\Delta T \; dt/dE|_{E_F}$ (where T is the average temperature, ΔT is the temperature difference across the junction, and t is a transmission coefficient depending on the carrier energy E), and hence to decrease rapidly as the junction conductance $[G = (2e^2/h)t(E_F)]$ decreases. Our subject in this paper will be the symmetric PC peaks observed for narrow, high-resistance graphene nanoconstrictions in which the antisymmetric heating signal is suppressed.

The amplitude of the symmetric PC signals for the narrow graphene nanoconstrictions vary strongly as a function of the

dx.doi.org/10.1021/nl200522t |Nano Lett. 2011, 11, 1814–1818

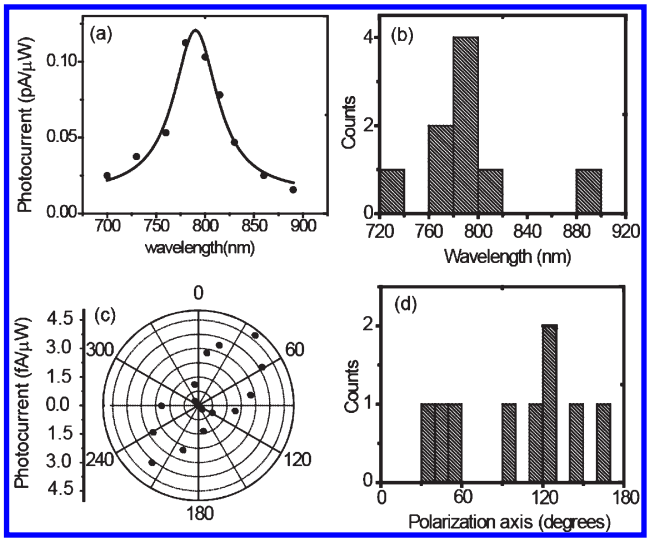

Figure 3. (a) Wavelength dependence of the photocurrent from device 6, showing a plasmon resonance at ~790 nm with a full width at half-maximum of 40 nm. (b) Histogram of the plasmon resonance peak frequencies in 9 devices. (c) Polarization dependence of the photocurrent for device 2 at 780 nm, plotted relative to the long axis of the gold wire. (d) Histogram of the polarization axes for maximum photocurrent response, relative to the long axis of the wire.

Table 1. Plasmon Enhancement of the Photocurrent Response Measured from the Peak-to-Background Ratio of the Resonance Curve versus Wavelength

device	R	resonance wavelength (nm)	PC enhancement
2	80 kΩ	780	3
4	160 kΩ	740	5
6	5 MΩ	790	7
7	25 MΩ	710	6
8	>50 GΩ	770	104

wavelength and polarization of the incoming light. Figure 3a shows the wavelength response of the PC for a ~5 MΩ contact at room temperature. The PC is sharply peaked at 790 nm, typical for the plasmon resonance of an Au nanostructure[35] with a full width at half-maximum of 40 nm. This line width is relatively sharp because we measure the plasmon resonance in the single gold break junction without line width broadening due to ensemble averaging. In different devices, we find that the plasmon peak varies over a range of 740−890 nm (Figure 3b), presumably due to differences in the break junction geometries. We can estimate a lower bound on the plasmon enhancement of the PC by comparing the peak value of the PC resonance to the value far into the tail (this is a lower bound since our ability to measure far into the tail is limited to the range shown by the wavelength tunability for our laser). For the device shown in Figure 3a, the plasmon enhancement factor of the PC is about 7. For other devices with room-temperature resistances in the range 50 kΩ to 5 MΩ, the PC enhancement factors vary from 2 to 7 (Table 1). Because the enhancement in the PC should go as the square of the enhancement in the local electric field (see below), the electric field enhancement factor by this method is a factor of 1.5−2.5. This variation likely reflects both that the strength of the true plasmon-enhanced electric field varies from devices to device, because, for example, the spacing between the gold electrodes is different, and also that the effect of the plasmon-enhanced electric field on the PC may depend on the precise position of the tunnel barrier in the device. The narrowest region of the graphene nanoconstriction will not necessarily be centered between the gold electrodes, and if it is closer to an electrode in some devices rather than others, this could strongly affect the sensitivity of photodetection.

The dependence of the PC on the polarization of the incoming light is shown for a different (R = 80 kΩ) device in Figure 3c. The PC varies strongly with the polarization angle in a simple dipole pattern with a factor of 11 variation from minimum to maximum response [equivalent to a polarization sensitivity $(PC_{max} - PC_{min})/PC_{max} + PC_{min} \sim 85\%$]. To the best of our knowledge, such a strong polarization dependence has not been demonstrated previously for nanogap electrodes acting as a plasmonic antenna. The polarization angle for maximum PC for the device in Figure 3c is 39° relative to the direction of the long axis of the gold wire. For different graphene constrictions in the range 50 kΩ to 5 MΩ, our polarization sensitivity varies from 50 to 85% and the polarization angle for maximum PC can lie in any direction in the sample plane with no apparent correlation to the long axis of the Au wire (Figure 3d). This may reflect the irregular geometry of junctions formed by electromigration, in which the orientation of the gap need not be aligned with the long axis of the wire.

As control devices, we studied both Au break junctions with no graphene and graphene nanoconstrictions without nanogap gold electrodes. Au break junctions without graphene do not produce any measurable photocurrent response. For graphene nanoconstrictions in which the nanogap Au electrodes are removed by a wet etch, we observe only the heating-type signals that are antisymmetric in sign as a function of spot position. These do not have a resonant dependence on wavelength in our tuning range from 700 to 980 nm.

As we have noted above, the sign of the PC peak that we observe in the high-resistance graphene nanoconstriction devices varies seemingly randomly from device to device. The simplest approach to explain the mechanism behind the photocurrent is to postulate that the optical-frequency voltage generated by the plasmon enhancement is rectified by the nonlinear electrical transport characteristic of the graphene device, which yields the prediction (in the regime that a lowest-order Taylor series in V_{opt} is accurate)

$$I_{PC} = \frac{1}{4}\frac{d^2I}{dV^2}V_{opt}^2 \qquad (1)$$

where V_{opt} is the plasmon-enhanced optical-frequency voltage dropped across the device and d^2I/dV^2 is calculated at the optical frequency. We have verified that I_{PC} has a simple linear dependence on the incident laser power in all of our devices, so that the lowest-order Taylor-series approximation is appropriate. Assuming that the tunneling time is short compared to the optical period,[12] we can test eq 1 by measuring the curvature d^2I/dV^2 at low frequency by conventional electrical transport techniques and checking whether the sign of d^2I/dV^2 is the same as I_{PC}. The curvature at room temperature near zero bias is not large (see Figure 1c inset); we can measure it using a lock-in amplifier with AC voltages ≤100 mV. The results are shown in Table 2. For five devices with resistances in the 25−180 kΩ range for which we have done this measurement, two showing positive PC and three

dx.doi.org/10.1021/nl200522t |Nano Lett. 2011, 11, 1814–1818

Table 2. Comparison of the Sign and Size of the Nonlinearity in the Current−Voltage Curve Measured Electrically with the Sign and Size of the Photocurrent

device	R	$1/4\ d^2I/dV^2$ (A/V^2)	PC (pA/μW)
1	25 kΩ	$(2.77 \pm 0.07) \times 10^{-6}$	2.51
2	80 kΩ	$(6 \pm 1) \times 10^{-7}$	0.0047
3	90 kΩ	$(-8 \pm 2) \times 10^{-6}$	−1.49
4	160 kΩ	$(-9 \pm 1) \times 10^{-7}$	−6.11
5	180 kΩ	$(-6 \pm 4) \times 10^{-7}$	−0.78

negative, the sign of d^2I/dV^2 agreed with the sign of the PC in each case. Assuming an electrode spacing of d = 3−10 nm, the values of the enhanced electric field $E_{opt} = V_{opt}/d$ derived from eq 1 and the measured values of d^2I/dV^2 are 1−20 times the bare value without plasmon enhancement ($E_{bare} = [2P/(\varepsilon_0 cA)]^{1/2}$, where P is the optical power, ε_0 is the permittivity constant, c is the speed of light, and A is the spot size).[36] The order of magnitude of the plasmon enhancement estimated from eq 1 is therefore consistent with the completely independent measurement of the enhancement based on the amplitude of the resonance curves as a function of wavelength. This reinforces our confidence both in these estimates and in our identification of optical rectification as the mechanism for the photocurrent.

Up to this point, we have discussed only devices with room-temperature resistances in the range 20 kΩ to 5 MΩ for which, based on the similarity of our $I-V$ curves to previous studies of graphene constrictions,[15−17,20−28] we conclude that the graphene remains physically continuous even though it possesses an energy gap that presents a tunnel barrier for electron flow. However, following the first stage electromigration-induced breaking of our Au wires, in about 1% of devices we observe much higher resistances (3 GΩ to >50 GΩ) for which we cannot tell whether the graphene is continuous or whether it might be fully broken or contain a grain boundary[37] or a crease. These devices can show much more dramatic plasmon enhancements than the lower-resistance graphene nanoconstrictions. Figure 4a shows the PC resonance curve for a device with R > 50 GΩ at room temperature. The peak-to-tail ratio yields a lower bound on the PC plasmon enhancement of 100 (electric field enhancement of 10). The polarization sensitivity (Figure 4b) for the same device is >99%. These devices were particularly sensitive to large incident laser powers; after the device in Figure 4 was exposed to a pulsed laser excitation of 100 mW peak power with 250 fs pulses, the PC reversed sign (Figure 4c,d). The resonant wavelength did not change significantly on account of this switch, but the polarization axis shifted by ∼20°. This switching indicates the high degree of sensitivity of the plasmon enhancement to the nanoscale atomic arrangements within the device.

In summary, we have demonstrated a self-aligned procedure for fabricating graphene nanoconstrictions coupled to gold nanogap plasmonic antennas so that the graphene device can perform direct electrical read-out of the enhanced electric field generated by the plasmon. Our integrated device structure allows us to characterize the wavelength and polarization dependence of the plasmon resonance in individual nanogap antennas, which has not been achieved previously. We find that the polarization dependence is particularly striking with polarization sensitivities as large as 99%, and that the polarization sensitivity and polarization axis both vary from device to device, presumably due to the irregular geometry of gold break junctions. This integration of plasmonic antennas with intrinsically nanoscale photodetectors for electrical readout provides a powerful platform for understanding how light energy may be controlled on small length scales and how the properties of plasmon resonances depend on nanoscale variations in device geometry.

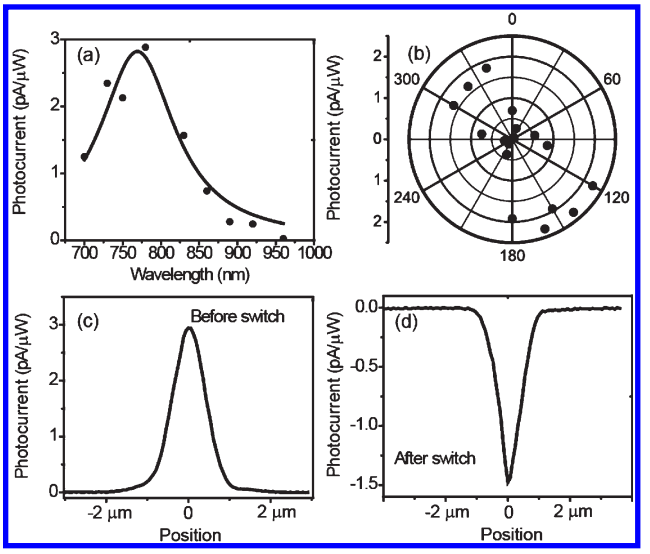

Figure 4. Photocurrent from a very high resistance device. (a) Wavelength dependence of the photocurrent of device 8 with room-temperature resistance >50 GΩ. (b) Polarization dependence of the photocurrent in the same device, demonstrating polarization sensitivity >99%. (c) A positive photocurrent signal before the device response switched under pulsed laser illumination. (d) Negative photocurrent signal after the device switched.

AUTHOR INFORMATION

Corresponding Author

*E-mail: ralph@ccmr.cornell.edu. Telephone: (607) 255-9644. Fax: (607) 255-6428.

ACKNOWLEDGMENT

We thank A. Mellnik and W. Li for assistance. This research was supported by the NSF (DMR-1010768), the Cornell Center for Chemical Interfacing, a Phase I Center for Chemical Innovation (NSF/CHE-0847926), and the Center for Nanoscale Systems (NSF/EEC-0646547). Device fabrication was performed at the Cornell Nanofabrication Facility/National Nanofabrication Infrastructure Network.

REFERENCES

(1) Gramotnev, D. K.; Bozhevolnyi, S. I. *Nat. Photonics* **2009**, *3*, 55.
(2) Schuller, J. A.; Barnard, E. S.; Cai, W.; Jun, Y. C.; White, J. S.; Brongersma, M. L. *Nat. Mater.* **2010**, *9*, 193.
(3) Campion, A.; Kambhampati, P. *Chem. Soc. Rev.* **1998**, *27*, 241.
(4) Nie, S.; Emory, S. R. *Science* **1997**, *275*, 1102.
(5) Ward, D. R.; Halas, N. J.; Ciszek, J. W.; Tour, J. M.; Wu, Y.; Nordlander, P.; Natelson, D. *Nano Lett.* **2008**, *8*, 919.
(6) Schuck, P. J.; Fromm, D. P.; Sundaramurthy, A.; Kino, G. S; Moerner, W. E. *Phys. Rev. Lett.* **2005**, *94*, 017402.
(7) Kim, S.; Jin, J.; Kim, Y.-J.; Park, I.-Y.; Kim, Y.; Kim, S.-W. *Nature* **2008**, *453*, 757.
(8) Muhlschlegel, P.; Eisler, H.-J.; Martin, J. F.; Hecht, B.; Pohl, D. W. *Science* **2005**, *308*, 1607.

(9) Kinkhabwala, A.; Yu, Z.; Fan, S.; Avlasevich, Y.; Müllen, K.; Moerner, W. E. *Nat. Photonics* **2009**, *3*, 654.
(10) Kuhn, S.; Hakanson, U.; Rogobete, L.; Sandoghdar, V. *Phys. Rev. Lett.* **2006**, *97*, 017402.
(11) Song, J.-H.; Atay, T.; Shi, S.-F.; Urabe, H.; Nurmikko, A. V. *Nano Lett.* **2005**, *5*, 1557.
(12) Ward, D. R.; Hüser, F.; Pauly, F.; Cuevas, J. C.; Natelson, D. *Nat. Nanotechnol.* **2010**, *5*, 732.
(13) Li, X.; Cai, W.; An, J.; Kim, S.; Nah, J.; Yang, D.; Piner, R.; Velamakanni, A.; Jung, I.; Tutuc, E.; Banerjee, S. K.; Colombo, L.; Ruoff, R. S. *Science* **2009**, *324*, 1312.
(14) Strachan, D. R.; Smith, D. E.; Johnston, D. E.; Park, T.-H.; Therien, M. J.; Bonnell, D. A.; Johnson, A. T. *Appl. Phys. Lett.* **2005**, *86*, 043109.
(15) Standley, B; Bao, W.; Zhang, H.; Bruck, J.; Lau, C. N.; Bockrath, M. *Nano Lett.* **2008**, *8*, 3345.
(16) Moser, J.; Bachtold, A. *Appl. Phys. Lett.* **2009**, *95*, 173506.
(17) Lu, Y.; Goldsmith, B.; Strachan, D. R.; Jim, J. H.; Luo, Z. T.; Johnson, A. T. *Small* **2010**, *6*, 2748.
(18) Murali, R.; Yang, Y.; Brenner, K.; Beck, K.; Meindl, J. D. *Appl. Phys. Lett.* **2009**, *94*, 243114.
(19) Moser, J.; Bachtold, A. *Appl. Phys. Lett.* **2009**, *95*, 173506.
(20) Han, M. Y.; Özyilmaz, B.; Zhang, Y.; Kim, P. *Phys. Rev. Lett.* **2007**, *98*, 206805.
(21) Chen, Z.; Lin, Y.-M.; Rooks, M. J.; Avouris, P. *Physica E* **2007**, *40*, 228.
(22) Ponomarenko, L. A.; Schedin, F.; Katsnelson, M. I.; Yang, R.; Hill, E. W.; Novoselov, K. S.; Geim, A. K. *Science* **2008**, *320*, 356.
(23) Stampfer, C.; Güttinger, J.; Hellmüller, S.; Molitor, F.; Ensslin, K.; Ihn, T. *Phys. Rev. Lett.* **2009**, *102*, 056403.
(24) Todd, K.; Chou, H.-T.; Amasha, S.; Goldhaber-Gordon, D. *Nano Lett.* **2009**, *9*, 416.
(25) Liu, X.; Oostinga, J. B.; Morpurgo, A. F.; Vandersypen, L. M. K. *Phys. Rev. B* **2009**, *80*, 121407(R).
(26) Gallagher, P.; Todd, K.; Goldhaber-Gordon, D. *Phys. Rev. B* **2010**, *81*, 115409.
(27) Han, M. Y.; Brant, J. C.; Kim, P. *Phys. Rev. Lett.* **2010**, *104*, 056801.
(28) Li, X.-L.; Wang, X.; Zhang, L.; Lee, S.; Dai, H. *Science* **2008**, *319*, 1229.
(29) Ritter, K. A.; Lyding, J. W. *Nat. Mater.* **2009**, *8*, 235.
(30) Tang, L.; Kocabas, S. E.; Latif, S.; Okyay, A. K.; Ly-Gagnon, D.-S.; Saraswat, K. C.; Miller., D. A. B. *Nat. Photonics* **2008**, *2*, 226.
(31) Pérez-González, O.; Zabala, N.; Borisov, A. G.; Halas, N. J.; Nordlander, P.; Aizpurua, J. *Nano Lett.* **2010**, *10*, 3090.
(32) Park, J.; Ahn, Y. H.; Ruiz-Vargas, C. *Nano Lett.* **2009**, *9*, 1742.
(33) Xu, X.; Gabor, N. M.; Alden., J. S.; Van der Zande, A. M.; McEuen, P. L. *Nano Lett.* **2010**, *10*, 562.
(34) van Houten, H.; Molenkamp, L. W.; Beenakker, C. W. J.; Foxon, C. T. *Semicond. Sci. Technol., B* **1992**, *7*, B215.
(35) Auguié, B.; Barnes, W. L. *Phys. Rev. Lett.* **2008**, *101*, 143902.
(36) Jackson, J. D. *Classical electrodynamics*; Wiley: New York, 1998.
(37) Yazyev, O. V.; Louie, S. G. *Nat. Mater.* **2010**, *9*, 806.